Feasibility of human spinal cord perfusion mapping using dynamic susceptibility contrast imaging at 7T: Preliminary results and identified guidelines

Simon Lévy, Pierre-hugues Roche, Maxime Guye, Virginie Callot

Feasibility of human spinal cord perfusion mapping using Dynamic Susceptibility Contrast imaging at 7T: preliminary results and identified guidelines

Simon Lévy[1-4], Pierre-Hugues Roche[4,5], Maxime Guye[1,2], Virginie Callot[1,2,4]

Affiliations

[1] Aix-Marseille Univ, CNRS, CRMBM, Marseille, France

[2] APHM, Hopital Universitaire Timone, CEMEREM, Marseille, France

[3] Aix-Marseille Univ, Univ Gustave Eiffel, LBA, Marseille, France

[4] iLab-Spine International Associated Laboratory, Marseille-Montreal, France-Canada

[5] APHM, Hopital Nord, Neurosurgery Department, Marseille, France

Corresponding author

Virginie Callot

CRMBM-CEMEREM, UMR 7339, CNRS, Aix-Marseille Université

27 bd Jean Moulin

13385 Marseille cedex 05, France

Office: +334 91 38 84 65 | Email: virginie.callot@univ-amu.fr

Word count for body of the text: 3908

Abstract

Purpose: To explore the feasibility of Dynamic Susceptibility Contrast (DSC) MRI at 7T for human spinal cord (SC) perfusion mapping and fill the gap between brain and SC perfusion mapping techniques.

Methods: Acquisition protocols for high-resolution single-shot EPI in the SC were optimized for both spin-echo and gradient-echo preparations, including cardiac gating, acquisition times and breathing cycle recording. Breathing-induced MRI signal fluctuations were investigated in healthy volunteers. A specific image and signal processing pipeline was implemented to address them.

DSC was then evaluated in 3 healthy volunteers and 5 patients. Bolus depiction on slice-wise signal within cord was investigated and maps of relative perfusion indices were computed.

Results: Signal fluctuations were increased by 1.9 and 2.3 in free breathing compared to apnea with spin-echo and gradient-echo, respectively. The ratio between signal fluctuations and bolus peak in healthy volunteers was 5.0% for spin-echo and 3.8% for gradient-echo, allowing clear depiction of the bolus on every slice and yielding relative blood flow and volume maps exhibiting the expected higher perfusion of gray matter.

However, in patients, signal fluctuations were increased by 4 in average (using spin-echo), compromising the depiction of the bolus in slice-wise signal. Moreover, 3/18 slices had to be discarded because of fat aliasing artifacts.

Conclusion: DSC MRI at 7T showed great potential for SC perfusion mapping with a reliability never achieved so far for single-subject and single-slice measurements. Signal stability needs to be improved in acquisition conditions associated with patients but guidelines to achieve that were identified and shared.

Keywords: spinal cord, dynamic susceptibility contrast, DSC MRI, 7T MRI, perfusion, ultrahigh field MRI

1. Introduction

Blood perfusion is frequently involved in spinal cord (SC) injuries[1,2]. Indeed, a prolonged SC compression such as in traumas may result in a local reduction of tissue perfusion and progressive ischemia, leading to metabolism alteration and potentially irreversible tissue necrosis[3]. In such case, perfusion recovery is conditional to clinical presentation improvement. Similarly, in non-traumatic disorders such as Cervical Spondylotic Myelopathy (CSM), chronic SC compression may progressively induce ischemia[4]. Unfortunately, today, there is a critical lack of technique to confidently assess SC perfusion status.

By contrast, in the brain, several techniques such as Arterial Spin Labeling (ASL)[5], Intra-Voxel Incoherent Motion (IVIM)[6] or the reference technique in clinics, Dynamic Susceptibility Contrast (DSC) MRI, can now provide reliable blood volume and blood flow maps of patients with white (WM) and gray (GM) matter distinction. Such maps are an important tool for clinicians to assess the extent of ischemic stroke for instance[7]. From a clinical point of view, SC perfusion maps would be valuable to assess the extent and progression of perfusion deficit and identify the specific functional area at stake. From a technical point of view, regional mapping of SC perfusion with high resolution would also be a way to assess the reliability of the measurements. Indeed, a similar GM/WM perfusion difference in brain and SC is expected (based on microangiography[8], histology[9] and ASL in mice[10]).

However, the transfer of the techniques used in brain to SC is not trivial. Indeed, its location in the vicinity of lungs, directly surrounded by pulsatile Cerebrospinal Fluid (CSF), is source of multiple biases and artifacts. In particular, breathing-induced field fluctuations have shown a significant effect on MRI signal, even at the cervical level[11,12]. Moreover, its size (~8x13mm^2 in transverse section) requires high resolution to allow GM depiction. An additional challenge, similar to the brain[10,13], is the low perfusion level compared to other organs (e.g. kidneys, liver, heart), with GM being more perfused than WM[10,14].

Among endogenous methods, ASL has been experimented at 1.5T[15] and 3T[16] for SC perfusion mapping. However, only poor sensitivity and reliability were obtained. IVIM was evaluated at 7T, but sensitivity at single-subject and single-slice scale was limited and averaging across multiple subjects (≥6) was necessary to map the perfusion difference between GM and WM[17].

Very little literature exists regarding contrast agent-based perfusion MRI techniques in the human spinal cord. Vascular-Space-Occupancy (VASO) MRI has been used to map the absolute SC blood volume (BV) in healthy subjects[13]. A mean value of 4.3mL/100mL tissue was obtained with a good reproducibility across field strengths (1.5 and 3T). However, this technique does not provide blood flow-relative metrics. In addition, inflowing fresh blood[18] and CSF volume changes[19] were shown to affect VASO MRI measurements. Later, example maps of tissue permeability metrics obtained with Dynamic Contrast-Enhanced MRI in a patient with spinal cord glioblastoma were published as part of a review[20]. Although tumors involve abnormally increased perfusion levels, no blood flow or blood volume map was obtained with this technique either. However, DSC MRI, which requires a higher temporal resolution, recently showed promising sensitivity at 3T in CSM patients where ischemia is expected[21]. Indeed, relative SC BV was negatively correlated to cord compression and decreased with symptoms severity as assessed by clinical tests[22]. However, those results were obtained at the group level through multiple voxel- and slice-averaged perfusion measurements, with coarse resolution, which helped sensitivity but excluded individual and regional perfusion mapping, limiting the clinical impact. In this exploratory study, we aimed to assess the potential of DSC MRI for regional perfusion-related indices mapping at the individual scale.

To cope with the high-resolution necessary to GM and WM imaging in SC, the investigations were performed at 7T, which is now becoming a clinical tool[23–25]. Higher field strength theoretically provides higher SNR but also increases susceptibility effects, which is expected to provide an increased sensitivity to gadolinium-based contrast agent bolus in DSC imaging[26,27]. However, higher field strength also comes with new challenges. Sensitivity to susceptibility variations and resulting B0 inhomogeneity/fluctuations is increased. B1 transmission ($B1^+$) and reception ($B1^-$) are more limited and heterogeneous. Such features have significant consequences in the SC physiological environment. The feasibility and sensitivity of DSC MRI at 7T for human spinal cord perfusion mapping were therefore investigated.

2. Methods

All acquisitions were performed on a 7T whole-body research system (Magnetom, Siemens Healthcare, Erlangen, Germany) using a commercial 8-channel cervical-spine transceiver surface coil (Rapid Biomedical GmbH, Rimpar, Germany) with the 8 Tx-channels hardware-combined into a single transmit system.

2.1. Acquisition parameters

Acquisitions were cardiac gated (pulse oximeter) to mitigate cord motion with CSF pulsations. A single-shot two-dimensional EPI readout was employed given the high temporal resolution required, determined by the cardiac beat. Physiological Monitoring Unit (PMU) was activated in the sequence code to allow acquisition time stamp recordings, further used for post-processing normalization by effective TR. A respiratory belt was placed either on the subject's abdomen or chest (depending on her/his main mode of breathing) to record breathing cycles during acquisition.

DSC can be performed using either gradient-echo sequence based on the change $\Delta R2^*$ in R2* relaxation rate, or spin-echo sequence looking at the change $\Delta R2$ in R2 relaxation rate. Both types of sequences were investigated.

An in-plane resolution of $0.7\times0.7mm^2$ was aimed for, which was obtained with truncated FOV coming with aliasing at the edges but far from the cord. Acquisitions were also performed with a coarser resolution ($1.0\times1.0mm^2$) allowing the FOV to include the whole neck cross-section. Fat saturation was used without outer volume suppression. Slice thickness was set to 5mm. An acceleration factor of 2 (GRAPPA) was used. Automatic calibration scans, partial Fourier and TE were single-shot EPI, 6/8 and 42ms for the spin-echo sequence, and gradient-echo FLASH, 5/8 and 22ms for the gradient-echo sequence, respectively.

Acquisitions so far were limited to 3 slices (one by vertebral level, see Supporting Information Figure S1) because of the Specific-Absorption-Rate (SAR) restrictions associated with spin-echo and TR around 800-1100ms (cardiac cycle). To optimize SNR with regards to the subject's cardiac cycle (effective TR), when allowed by SAR limits, excitation flip angle was set to the corresponding Ernst angle (or 180^o – Ernst angle for spin-echo), with TR being the mean cardiac cycle duration and T_1 the mean longitudinal relaxation time in healthy SC tissue at 7T (1251ms[28]).

2.2. In-vivo evaluation

The study was approved by the local ethics committee and written consents were obtained from all participants prior to MR examinations.

First, the effects of breathing on signal stability were investigated within 5 healthy volunteers (2 with spin-echo, 2 with gradient-echo and 1 with both sequences). Participants were asked to breath-in, hold their breath and then, the acquisition was started to make sure that automatic calibration scans were acquired during breath-hold. Participants were asked to slowly release the breath-hold when they could not hold it any longer. Data were compared with free breathing condition and the temporal standard-deviation (tSD) of $\Delta R2^{(*)}$ ($\Delta R2$ for spin-echo, $\Delta R2^{*}$ for gradient-echo) was used to quantify signal stability.

Then, 3 healthy volunteers and 5 patients with CSM were recruited for evaluation of the technique with gadolinium injection. Each participant's characteristics are presented in Table 1. One of the patients was scanned before and after decompression surgery. The acquisition protocol included:

- $B1^{+}$ map: sagittal 2D saturation-prepared turbo-flash with $1.0\times1.0mm^2$ in-plane resolution, 5mm slice-thickness
- Sagittal anatomical imaging to refine slice position: 2D turbo spin-echo with $0.6\times0.6mm^2$ in-plane resolution, 2.2mm slice thickness
- B_0 map: sagittal 2D spoiled gradient-echo with $1.35\times1.35mm^2$ in-plane resolution, 5mm slice-thickness
- Transversal anatomical imaging for WM/GM depiction: 2D multi-echo gradient-echo FLASH images with $0.4\times0.4mm^2$ in-plane resolution, 5mm slice-thickness, same slice position as for perfusion imaging.
- Perfusion imaging:

  Shimming was performed in a rectangular box, positioned longitudinally to the cord (~$4\times3\times9cm^3$ along Right-Left×Anterior-Posterior×Inferior-Superior axes); a full-width-at-half-maximum ≤100Hz and $T2^{*}$ ≥5ms were targeted.

  - DSC sequence (without injection) with reverse (left > right) phase-encoding direction (further used for post-processing distortion correction), 100 repetitions.

- DSC sequence with forward (right > left) phase-encoding direction, 220 repetitions, with injection after 70 repetitions (Dotarem, Guerbet, 0.2mL/kg, 5mL/s, followed by 30mL saline flush).

For perfusion imaging, spin-echo was employed in all patients and one healthy volunteer (HC1), while gradient-echo was used in the two other healthy volunteers (HC2, HC3). Acquisition time for perfusion imaging was ~4 minutes depending on the subject's heartbeat, while the complete protocol lasted ~35 minutes.

2.3. Data post-processing

The following image processing pipeline was set up for DSC data:

1) Gibbs artifacts were removed using the sub-pixel shifting method[29] (only for high-resolution acquisitions).
2) A rigid motion correction was applied slice-by-slice across repetitions using *ANTs*[30] with the accumulated mean across registered images as reference (starting from first repetition).
3) Denoising was applied with nonlocal transform-domain filter[31] (only for high-resolution acquisitions).

Steps 1 to 3 were applied to both reversed and forward phase-encoded series.

4) Distortion correction was applied with *Topup*[32] based on the temporal mean of the reversed and forward phase-encoded series.

Then, a specific signal processing pipeline was implemented in Python 3.6 as described below. The effects of each step (steps 5 to 8) can be observed in Figure 1.

5) Effective TR normalization: point-wise division by $1 - e^{-TR_{eff}/T_1}$ with TR_{eff} the effective TR retrieved from the PMU and T_1 the average T1 value in SC at 7T according to the available literature[28].
6) Discard inconsistent TRs: data acquired after a missed trigger and the following repetition were discarded from analysis because of steady-state loss (the first two repetitions were therefore also discarded).
7) Breathing frequencies filtering: a band-stop filter (Butterworth) was applied using the minimum and maximum breathing frequencies measured with the respiratory belt as cut-offs.
8) Final smoothing: a Savitzky-Golay filter with window length of 23 and a 5^{th}-order polynomial was applied. Special care was taken not to smooth out the bolus peak. This

parameter set yielded a good trade-off between smoothing of residual signal oscillations and bolus conservation for all subjects.

The code and a dataset have been made publicly available here: github.com/slevyrosetti/7T-DSC-MRI-Toolbox.

2.4. Data quality assessment

Native image series (both with forward and reverse phase encoding) were visually inspected in comparison to transversal anatomical multi-echo gradient-echo FLASH images to assess image distortion and spot any artifacts. Artifacts frequently encountered in high-resolution EPI of the SC – namely Nyquist N/2 ghosting, large signal dropout (mainly with gradient-echo sequences) or fat aliasing – are illustrated in Figure 2. Slices with artifacts reaching the cord were discarded.

2.5. Quantification of relative perfusion indices

Relative perfusion indices were quantified as follows:

1) Signal was converted to $\Delta R_2^{(*)}$ (s^{-1}): $\Delta R_2^{(*)}(t) = -\ln\left(\frac{S(t)}{S_0}\right).\frac{1}{TE}$ where S_0 is the mean signal across repetitions before injection.
2) A gamma-variate function was fitted to $\Delta R_2^{(*)}(t)$ based on the algorithm proposed in the *DSC-MRI-toolbox* (github.com/marcocastellaro/dsc-mri-toolbox).
3) Relative Blood Flow (rBF) was measured as the maximum slope of the curve, relative Blood Volume (rBV) as the area under the curve, Bolus Arrival Time (BAT) as the time between injection and bolus arrival, and Time-To-Peak (TTP) as the time between bolus arrival and bolus peak.

Depending on the study case, this routine and the preceding signal processing pipeline were performed either on mean signal in cord across the three slices, slice-wise or voxel-wise.

3. Results

3.1. Single-shot EPI image quality

Figure 2 compares the image quality of spin-echo and gradient-echo EPI within a healthy volunteer. Large signal dropout at the periphery of the SC can be observed with gradient-echo. Based on the anatomical gradient-echo FLASH image, gradient-echo EPI showed larger image distortions compared to spin-echo. Figure 2 also shows typical artifacts of high-resolution single-shot EPI. Nyquist N/2 ghosting artifacts could usually be addressed with a better shimming if achievable (not trivial). Among all datasets, 3/27 slices in total had to be discarded because of fat aliasing artifacts. The effects of the GRAPPA calibration scan mode and phase correction algorithms used can be observed in the last row of Figure 2 for acquisition in phantoms. Although it is the default option in most product sequences, single-shot EPI GRAPPA calibration does not seem optimal to avoid Nyquist N/2 ghosting. The "local" phase correction, as often referenced by MRI manufacturers (estimation of a k-space phase line-dependent shift in addition to a global term), slightly improves image quality but the most substantial improvement is obtained when using multi-shot versus single-shot EPI for the GRAPPA calibration.

3.2. Effect of breathing

Figure 3 compares the signal stability between apnea and free breathing conditions, along with the free breathing signal after motion correction and breathing frequencies filtering, both with spin-echo and gradient-echo preparation. Signal oscillations during free breathing are clearly mitigated during apnea. The mean tSD in cord (all slices) increased from $0.64s^{-1}$ in apnea to $1.22s^{-1}$ in free breathing (1.9-fold increase) with spin-echo, and from 0.75 to $1.75s^{-1}$ (2.3-fold increase) with gradient-echo. Rigid motion correction and breathing filtering enabled a tSD of 0.65 and $0.90s^{-1}$ to be recovered, respectively. Breathing-induced signal fluctuations were higher with gradient-echo, which was expected given the higher sensitivity to susceptibility variations of the T2*-weighted signal. No clear slice-dependent effect of breathing stood out, either at the individual or group (3 subjects) level (Figure 3, right column).

3.3. In-vivo DSC results

Figure 4 presents the DSC results obtained with gadolinium injection in healthy volunteers. The contrast agent bolus was clearly visible in every subject. As expected, the

bolus peak obtained with spin-echo ($2.0s^{-1}$) was lower than with gradient-echo ($10.3s^{-1}$ in average across the subjects). However, signal stability was better with spin-echo (tSD of 0.10 vs $0.39s^{-1}$), in agreement with results in Figure 3, yielding a ratio tSD/peak of 5.0% with spin-echo and 3.8% with gradient-echo. Bolus profiles in GM and WM can be found in Supporting Information Figure S2. Regarding mapping potential, the technique provided clear rBF maps, exhibiting the expected higher perfusion values of GM compared to WM, in agreement with the anatomical images shown alongside. Comparing spin-echo to gradient-echo for high-resolution ($0.7\times0.7mm^2$) maps, less distortions were obtained with spin-echo, as evidenced by the anatomical images which are free of distortions (e.g., most superior slice). The bolus peak observed in the high-resolution gradient-echo acquisition was higher than with the low-resolution ($1.0\times1.0mm^2$) acquisition (11.7 vs $8.8s^{-1}$). Interpretations about the effect of the resolution or about potential variations in perfusion values along the inferior-superior axis are nonetheless too preliminary at this stage.

Results in patients are presented in Figure 5. All patients' data were acquired with the spin-echo sequence. Individual slice-wise plots showed generally more signal fluctuations in baseline with patients than with healthy volunteers. In particular, for PATIENT 2, signal fluctuations were on the same order of magnitude as the bolus. However, the bolus was still visible in most cases but with different profiles: for instance, the boluses seem shared between two peaks in PATIENTS 2, 3 and 4. The hypothesis that this difference in bolus profile was due to the patients' cord compression and reflected a pathological perfusion condition needs to be verified but cannot be discarded. PATIENT 5, who had received decompression surgery, moved right after the injection (hence the multiple missed triggers); nevertheless, the bolus showed a more standard profile. Motion was probably the reason why signal did not come back to baseline after injection. Last row of Figure 5 compares the signal profiles in whole cord (all slices averaged) between all patients and HC1 (green line). In average across patients (discarding PATIENT 5 who had surgery), the mean bolus peak had the same amplitude as in HC1 ($2.0s^{-1}$), although timings and profile generally differed. However, the tSD in baseline was more than 4 times higher (0.44 vs. $0.1s^{-1}$ in HC1), yielding a tSD of the order of gradient-echo EPI in healthy volunteers and a ratio tSD/peak of 22%.

Finally, to illustrate the potentials of DSC in the human SC, Figure 6 shows maps of different perfusion-related indices obtained in healthy volunteer HC1 and two patients (with different in-plane resolutions). rBF and rBV maps depicted the higher perfusion values of GM compared to WM. Less difference could be observed between the two tissues

with timing indices, BAT and TTP, which showed relatively homogeneous values in the cord. The GM/WM ratios obtained in average in all three healthy volunteers (HC1, HC2, HC3) were 2.2, 1.6, 1.4 and 1.0 for rBF, rBV, BAT and TTP respectively (with regions of interest defined on rBF and rBV maps, discarding voxels corrupted by partial voluming at the edge of the cord). They were respectively 2.2, 2.1, 0.4 and 1.0 in average across PATIENTS 1, 3 and 4 (only including slices where GM could be depicted on rBF and rBV maps, i.e. 4/9).

4. Discussion

This exploratory study investigated the feasibility and sensitivity of DSC MRI at 7T for perfusion mapping in the human SC, both in healthy volunteers and patients. Both spin-echo and gradient-echo sequences were considered. Effects of physiology on signal stability were characterized and specific protocol and pipeline were developed to address them. The depiction of the bolus was verified slice-wise in the cord and maps of rBF, rBV, BAT and TTP indices were produced.

4.1. Challenges and resulting guidelines

4.1.1. Static B0 inhomogeneities

Several challenges of DSC at 7T are associated with single-shot EPI of the SC. Indeed, this readout technique is extremely sensitive to B0 inhomogeneities. The latter can result in large distortions (Figure 2) due to accumulated phase errors along the readout. Spin-echo EPI is less sensitive than gradient-echo as the effects of those inhomogeneities are refocused. B0 inhomogeneities also affect the correction of the shift between odd and even phase lines, which can vary across the FOV. A "local" phase correction (as generally referenced by MRI manufacturers) – i.e., estimation of an individual shift per line in addition to a global shift for all lines – is therefore advised. GRAPPA calibration can also be affected by distortions. For that, multi-shot EPI (also referenced as FLEET[33]) or gradient-echo FLASH[34] based calibration should be preferred when available. Otherwise, in general, important efforts need to be spent on shimming (shim box adjustments, reiterated shim currents calculation, and even manual shim currents adjustments if needed) prior to imaging to achieve good high-resolution single-shot EPI quality at 7T in the SC.

4.1.2. Dynamic B0 fluctuations and signal instability

This study clearly showed that DSC in the SC at 7T is also challenged by signal fluctuations in time. Breathing-induced B0 fluctuations were first identified as a significant source of fluctuations, in agreement with previous studies[11,12]. Indeed, based on our data, signal fluctuations during free breathing were halved in apnea (divided by 1.9 with spin-echo and 2.3 with gradient-echo). In free breathing, the induced motion along the phase-encoding axis could be corrected with rigid correction but signal fluctuations attributable to variations in T2* dephasing remained. The filtering of breathing frequencies in the temporal signal, as recorded with a respiratory belt, showed good performance in the

dataset of this study but this method must be evaluated in more subjects to make sure that bolus peak does not get significantly smoothed. Moreover, it assumes a linear relationship between respiratory sensor and breathing-induced B0 fluctuations. However, several studies supported the hypothesis of a non-linear relationship[12,35–37], which could be the reason why this method was not efficient in all subjects. Informing the patient to the technique sensitivity to her/his breathing, such as with prior acquisition in apnea (which could further allow the estimation of the breathing contribution in the signal fluctuations for this specific patient) might also help. Asking for apnea during the approximate bolus period (~20s starting ~10-15s post-injection) is an additional option to be investigated but increased signal fluctuations when the subject takes her/his first breath and releases the breath-hold must be considered carefully.

B0 variations in time can also occur with patient motion. Although the induced "geometric" change can be corrected in post-processing, the signal intensity change would remain and result in a signal drift along time. Finally, B0 fluctuations along acquisition can cause image artifacts to be enhanced along time. In particular, as reported in MR angiography[38], it is common to see Nyquist N/2 ghosting mixed with GRAPPA artifacts exacerbated during the passage of the contrast agent. Coming in the FOV through multiple inlets in the neck, the contrast agent may modify the susceptibility in multiple points, which, depending on the shimming quality, might disturb the 7T B0 field and the GRAPPA reconstruction algorithm.

Cardiac beat is also a source of motion for SC and its direct surrounding environment, mainly CSF. Indeed, CSF pulsations induce complex cord motion along the inferior-superior axis and in the transversal plane[39,40]. This source of bias is expected to be addressed with cardiac gating targeting the quiescent window for acquisition. Nevertheless, CSF pulsations and resulting flow patterns might not be perfectly regular across cardiac cycles, which is likely to add dynamic B0 variations in the vicinity of the cord and increase the signal instability.

4.2. Potentials and perspectives of DSC MRI at 7T in the human spinal cord

The DSC technique was able to provide high-resolution maps of relative perfusion indices with a clear distinction between GM and WM perfusion (in agreement with existing literature[8–10,41]) in every individual slice within healthy volunteers and in slightly less than one third of the slices within patients. To the best of the authors' knowledge, such results have never been achieved so far. To date, only results at the group level based on

measurements averaged across multiple slices (~9) and voxels in cord, with coarse resolution (5-mm slices with 1.9x1.9mm^2 in-plane resolution) had been possible at clinical field strength (3T)[22], excluding individual and regional examinations. The current study, albeit preliminary, suggests a promising potential of DSC for reliable assessment of perfusion abnormalities in the SC, with an identification of affected pathways, and open the door to new clinical investigations on the involvement of perfusion in SC pathologies. Establishment of earlier biomarker of tissue degeneration are also a significant potential of the technique.

Regarding the comparison between spin-echo and gradient-echo preparations, even though gradient-echo has not been tested in patients yet, some comparison elements can already be stated. The aim of this work being to achieve reliable perfusion mapping of the spinal cord, spin-echo was first employed for its higher robustness to B0 heterogeneity and better EPI quality at 7T. Thanks to the refocusing pulse of spin-echo, image distortions and signal dropout with susceptibility effects are mitigated compared to gradient-echo. However, this refocusing pulse also comes with more energy deposition and SAR was an important limitation for the number of slices and the use of the optimal flip angles at 7T. Secondly, although it is too preliminary to draw conclusion on the ratio tSD/bolus peak for each preparation in healthy subjects, signal fluctuations in patients with spin-echo were increased by more than 4 as compared to healthy controls, compromising the sensitivity to bolus. These increased signal fluctuations in patients are thought to be related to (1) more irregular breathing patterns (see breathing period SDs in red in Figure 2), (2) a decreased coil sensitivity ($B1^-$ field) associated with generally longer distances between coil and SC (elderly subjects with generally larger morphology) and (3) a lower signal because of higher SAR restrictions making impossible to reach the optimal flip angle in the cord. Point (1) is likely to bias the estimation of breathing frequencies and consequently, compromise the efficacy of the filtering. Points (2) and (3) resulted in a lower signal and thus, an increased contribution of the physiological noise in the signal. The effect of deglutition on signal stability should also be investigated. Patients are often associated with more discomfort during acquisition than healthy volunteers. It is therefore important to dedicate more time to installation and information about SC MRI challenges. Those signal fluctuations would probably have been larger with gradient-echo, as suggested by results in Figure 3, but bolus peak is expected to be higher. So far, gradient-echo preparation was only evaluated in healthy volunteers. As expected, image quality was lessened but so were signal fluctuations with respect to bolus peak, suggesting a higher sensitivity of the technique. However, more

subjects are needed and future investigations on the performance of gradient-echo in patients will be essential.

The technical challenges related to ultrahigh field MRI are likely to be addressed in the coming years. Parallel transmission is a promising avenue to address SAR restrictions and $B1^+$ inhomogeneities. Design for SC coil arrays could be optimized to improve transmit and receive fields efficiency in a wider range of morphologies. A design with both anterior and posterior elements have already been proposed for cervical cord imaging at 7T[42]. Dynamic slice-wise shimming or real-time shimming such as SC coil arrays integrating real-time correction of breathing-induced B0 fluctuations[43] would further help to reduce distortions and signal instability. Finally, multiband acquisitions[44] with adequate coil design could be used to increase the number of slices and cover the whole cervical cord despite cardiac gating, but at the expense of SAR and SNR[45].

5. Conclusion

DSC at 7T showed great potential for perfusion mapping in the human SC within a clinical context, despite multiple challenges. In healthy volunteers, individual slice-wise maps of rBF and rBV were obtained, discriminating the GM perfusion from the WM, which, to the best of our knowledge, have never obtained so far. However, signal stability needs to be improved in acquisition conditions associated with patients. More investigations, especially using gradient-echo preparation, are needed but guidelines to ensure successful results could be identified and shared.

6. Tables

Table 1. Acquisition characteristics for each participant, healthy volunteers (HC) and patients. Slice positions for perfusion data and sagittal anatomical images (along with indications on spinal cord compressions in patients) can be found for each participant in Supporting Information Figure S1. SAR restrictions were calculated based on the reference voltage (required vs. set value) and the flip angle (Ernst angle vs. set value) within cord at the slice position of DSC acquisitions (SAR restrictions ≤10% implied that both the required reference voltage and optimal flip angle could be used). B0 inhomogeneities were assessed by measuring the maximum inter-slice frequency difference within cord. Favorable and disadvantageous characteristics for SAR restrictions and B0 inhomogeneities were highlighted in green and red, respectively. Particularly high SDs in the breathing period, which indicate more irregular breathing, were highlighted in red.

	Age / Sex	Body Mass Index	Mean ± SD cardiac period	Mean ± SD breathing period	SAR restrictions	Shortest cord<>coil distance	Maximum inter-slice frequency difference
HC 1	37 y.o. / Female	18.93 kg/m^2	903 ± 67 ms	4.1 ± 0.66 s	3.70 %	4.23 cm	63.8 Hz
HC 2	32 y.o. / Male	24.77 kg/m^2	1064 ± 56 ms	2.9 ± 0.49 s	15.31 %	5.32 cm	17.4 Hz
HC 3	33 y.o. / Male	24.57 kg/m^2	900 ± 54 ms	4.0 ± 0.52 s	2.45 %	4.44 cm	63.9 Hz
PATIENT 1	56 y.o. / Male	25.80 kg/m^2	865 ± 38 ms	3.5 ± 0.48 s	61.41 %	5.34 cm	47.8 Hz
PATIENT 2	68 y.o. / Male	26.51 kg/m^2	989 ± 28 ms	4.7 ± 1.37 s	50.63 %	5.64 cm	39.8 Hz
PATIENT 3	58 y.o. / Female	24.61 kg/m^2	900 ± 34 ms	4.8 ± 0.71 s	10.63 %	4.34 cm	32.3 Hz
PATIENT 4	43 y.o. / Male	24.68 kg/m^2	1178 ± 69 ms	3.5 ± 0.42 s	18.90 %	5.11 cm	38.6 Hz
PATIENT 5 (pre-surgery)	54 y.o. / Male	24.11 kg/m^2	901 ± 31 ms	4.4 ± 1.43 s	55.42 %	5.40 cm	10.4 Hz
PATIENT 5 (post-surgery)	55 y.o. / Male	27.44 kg/m^2	952 ± 68 ms	5.0 ± 2.04 s	18.25 %	4.35 cm	7.6 Hz

7. Figure

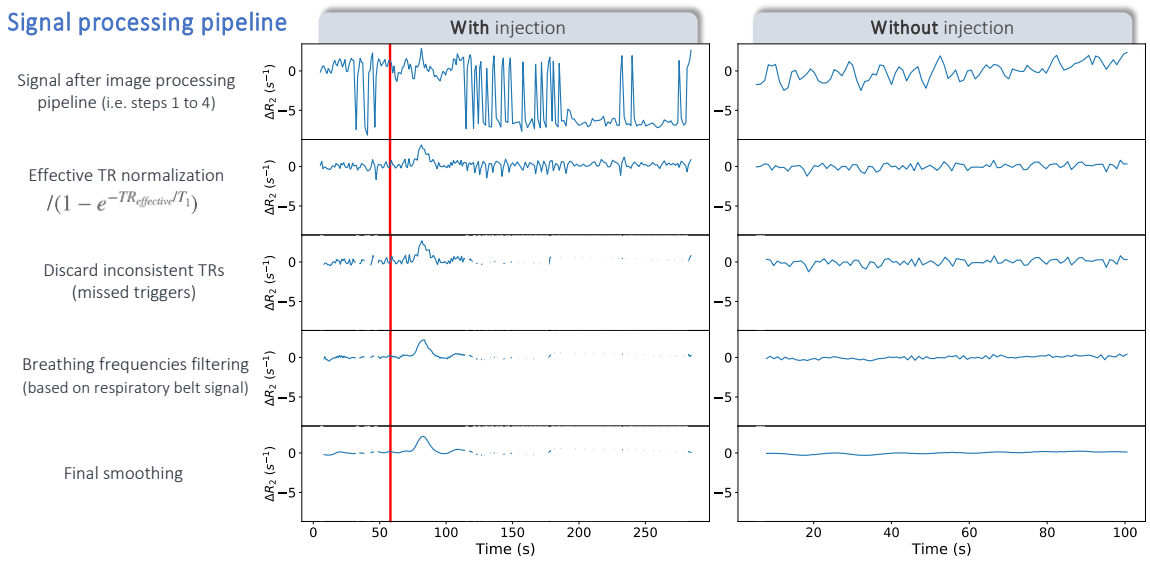

Figure 1. Signal processing pipeline illustrated on a dataset with gadolinium injection (left column, injection time indicated by the red line) **and without** (right column). The signal processing pipeline is applied directly after the image processing pipeline (steps 1 to 4 in Methods section 2.3). A case with multiple missed triggers has been specially chosen here for illustration purposes but only a few triggers were generally missed in the other datasets. The effect of those missed triggers can be visualized on the first line (left column) which plots the signal in a conservative region of interest within the cord (all slices averaged), along time: the steady-state loss yields large signal changes which are only partially corrected by the effective TR normalization (second line). Therefore, they need to be discarded (third line). The filtering of breathing frequencies (fourth line) removes most signal oscillations while keeping the bolus profile and peak, as does the final smoothing (last line) which filters out the remaining signal oscillations.

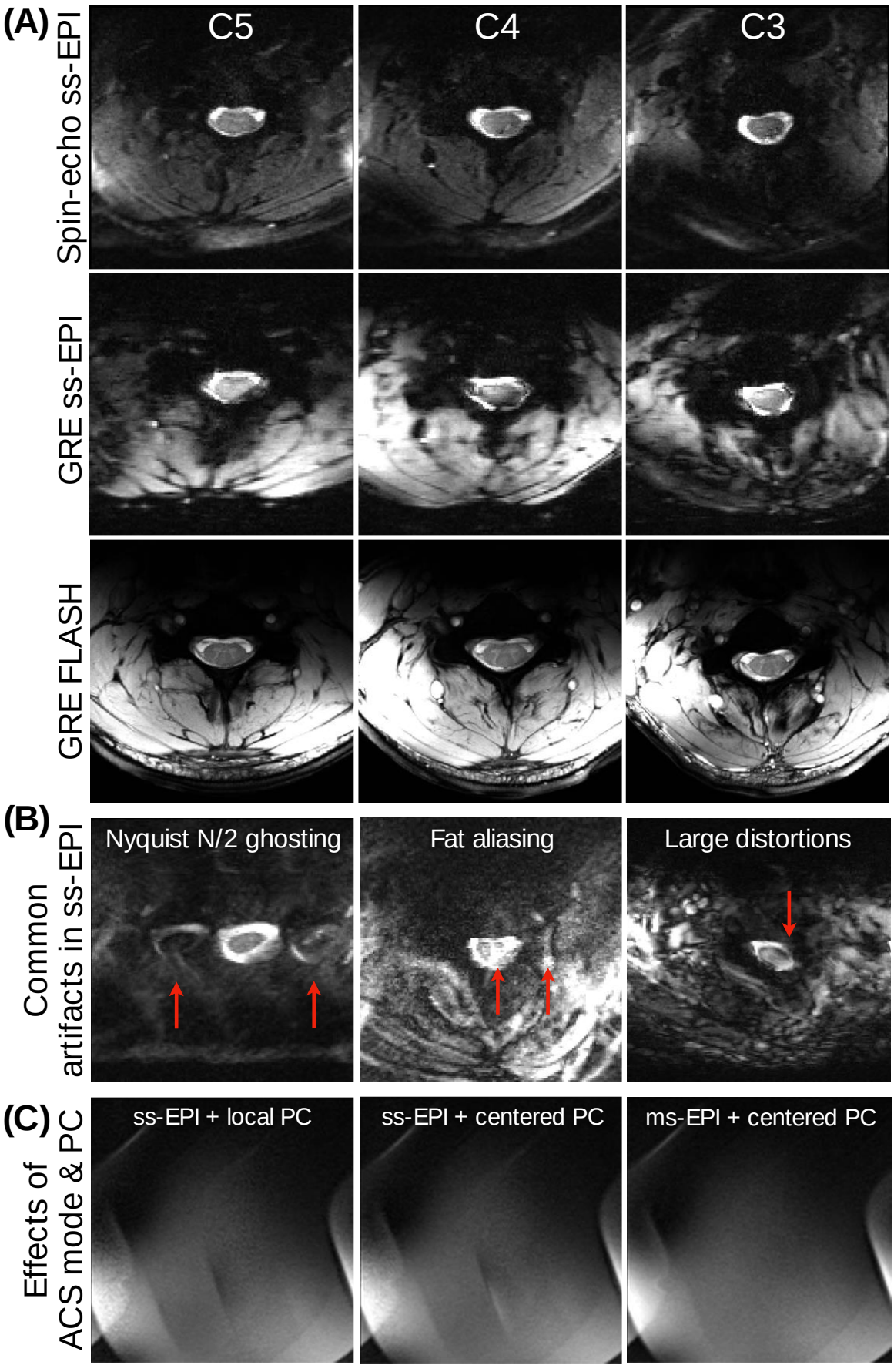
(A)
C5
C4
C3
Spin-echo ss-EPI
GRE ss-EPI
GRE FLASH
(B)
Common artifacts in ss-EPI
Nyquist N/2 ghosting
Fat aliasing
Large distortions
(C)
Effects of ACS mode & PC
ss-EPI + local PC
ss-EPI + centered PC
ms-EPI + centered PC

Figure 2. Image quality (A), common artifacts (B) and effects of GRAPPA calibration and EPI phase correction (C) in spin-echo and gradient-echo high-resolution single-shot EPI. (A): One repetition of spin-echo and gradient-echo (GRE) single-shot EPI (ss-EPI) with 0.7×0.7mm^2 in-plane resolution and 5-mm slice thickness within the same healthy volunteer (23-year-old man, example subject of Figure 3, not among the participants who received contrast agent injection). Comparison with the high-resolution anatomical multi-echo GRE FLASH image (first echo, 0.3×0.3mm^2, 5-mm slice thickness) enables the EPI-related image distortions to be evaluated. **(B):** Common artifacts (red arrows) obtained with high-resolution single-shot EPI (0.7×0.7mm^2, 5-mm slice thickness) in three different participants. **(C):** Effects on image quality of GRAPPA Automatic Calibration Scan (ACS) mode and phase correction algorithm obtained in phantom with spin-echo ss-EPI (0.7×0.7mm^2, 5-mm slice thickness): single-shot EPI (ss-EPI) vs. multi-shot EPI (ms-EPI) GRAPPA calibration and “local” vs. “centered” phase correction (PC). Local PC performed slightly better than centered PC although this improvement in image quality was minimal compared to the improvement provided by ms-EPI ACS calibration over ss-EPI.

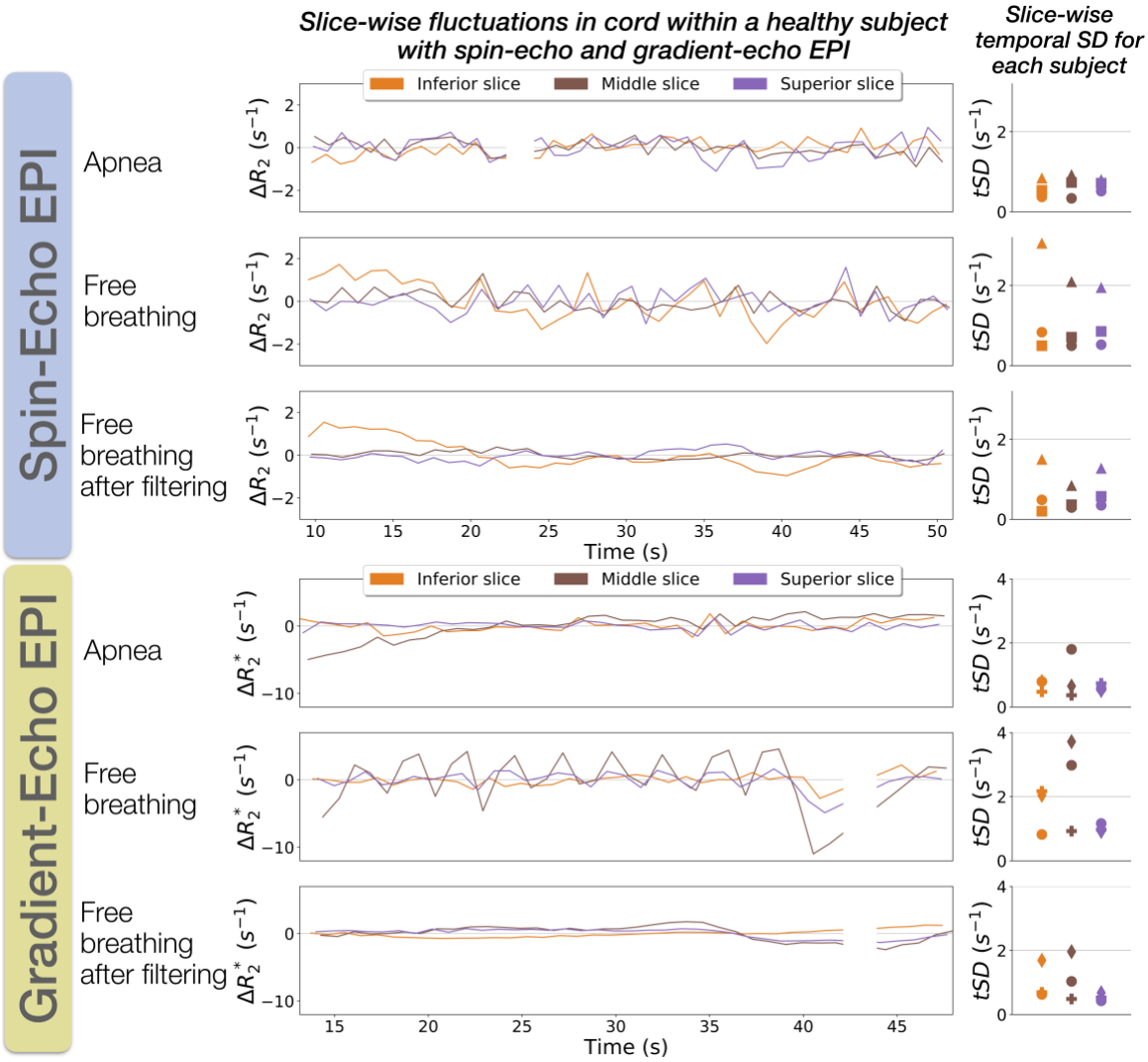

Figure 3. Breathing-induced signal fluctuations in spin-echo and gradient-echo high-resolution single-shot EPI. The plots show the evolution of the signal in a conservative region of interest in the spinal cord slice-by-slice, along time for spin-echo and gradient-echo acquisitions in the same healthy participant in apnea and free breathing. Graphs on the right-hand side show the temporal SD (tSD) by slice for each of the three subjects for inferior, middle and superior slices (represented in orange, brown and purple, respectively). Each marker represents a single subject; the data plotted in the middle graphs correspond to the subject represented with the circle marker on the right side. For a fair comparison, only rigid motion correction and breathing frequencies (as measured with the respiratory belt) were applied to free breathing data (leading to the row "Free breathing after filtering"). Also, note that the scales of the plots y-axes were adjusted independently for spin-echo and gradient-echo data (larger for gradient-echo) to allow the breathing-induced fluctuations to be visualized despite the different amplitudes.

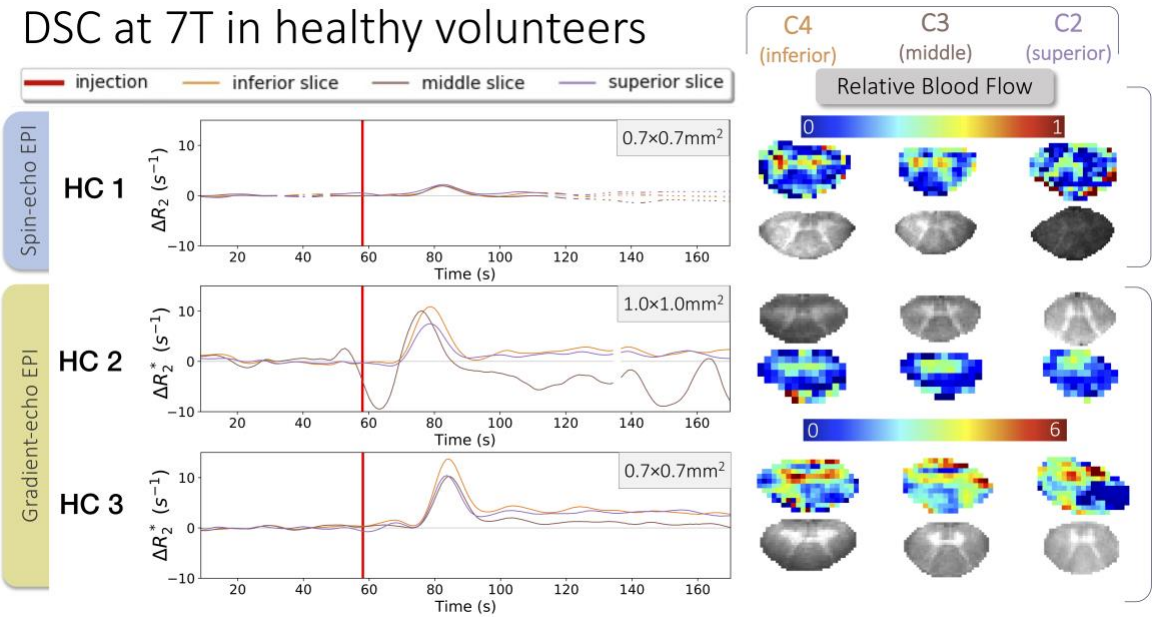

Figure 4. DSC results in 3 healthy volunteers at 7T. On the left side, the signal averaged within a conservative region of interest in the whole cord is plotted by slice along time. On the right side, the relative Blood Flow (rBF) maps resulting from a voxel-wise processing are presented alongside the corresponding anatomical scans (2D multi-echo gradient-echo FLASH with 0.4×0.4mm^2 in-plane resolution) for gray and white matter depiction. Spin-echo EPI was tested in one healthy volunteer with high in-plane resolution (0.7×0.7mm^2) while gradient-echo EPI was tested in two healthy volunteers, with high and lower (1.0×1.0mm^2) in-plane resolution.

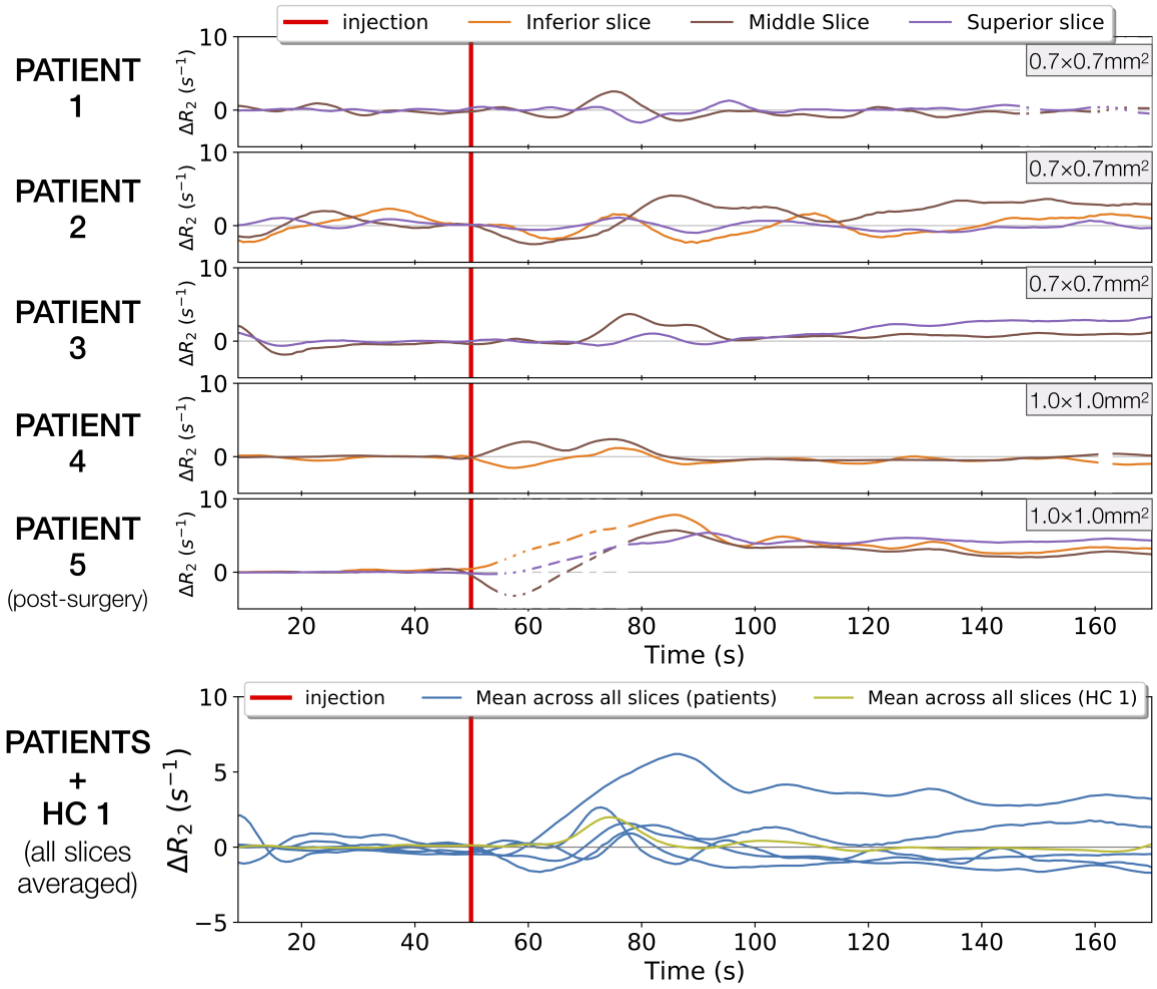

Figure 5. DSC results in 5 patients at 7T. The last row plots the signal in cord (all slices averaged) along time, for every patient in blue, and for the healthy volunteer (HC1) in green. Other rows are individual slice-wise plots of patients. All data acquired in patients were spin-echo EPI data. The in-plane resolution is indicated on the top right-hand corner of each plot.

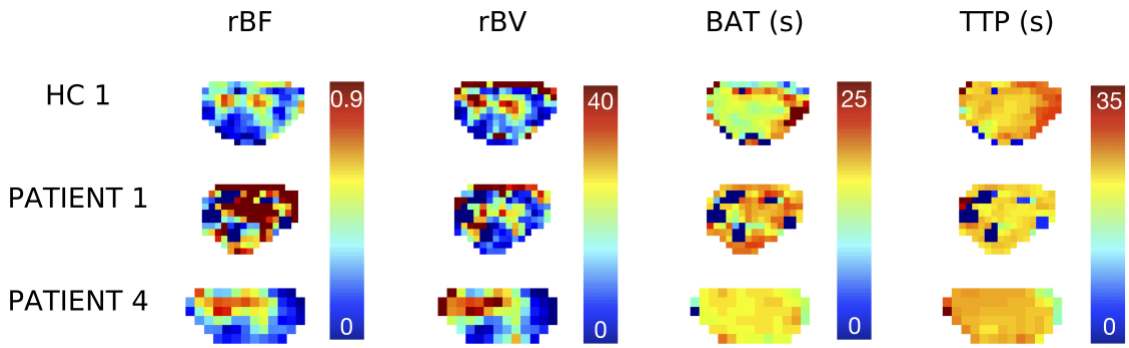

Figure 6. Examples of perfusion-related index maps that can be obtained from DSC in spinal cord at 7T: relative Blood Flow (rBF), relative Blood Volume (rBV), Bolus Arrival Time (BAT) and Time-To-Peak (TTP). Presented maps correspond to the middle slice of spin-echo DSC acquisitions with 0.7×0.7mm^2 in-plane resolution (HC 1, PATIENT 1) and with 1.0×1.0mm^2 in-plane resolution (PATIENT 4). For each perfusion index, colormaps were set to the same range for an easier comparison across subjects.

8. Supplementary Information

Filename	Description
Supporting Information.pdf	**Supporting Information Figure S1:** Sagittal anatomical images and slice positions for cervical cord perfusion imaging **Supporting Information Figure S2:** DSC results in 3 healthy volunteers at 7T with gray and white matter signal-time profiles.

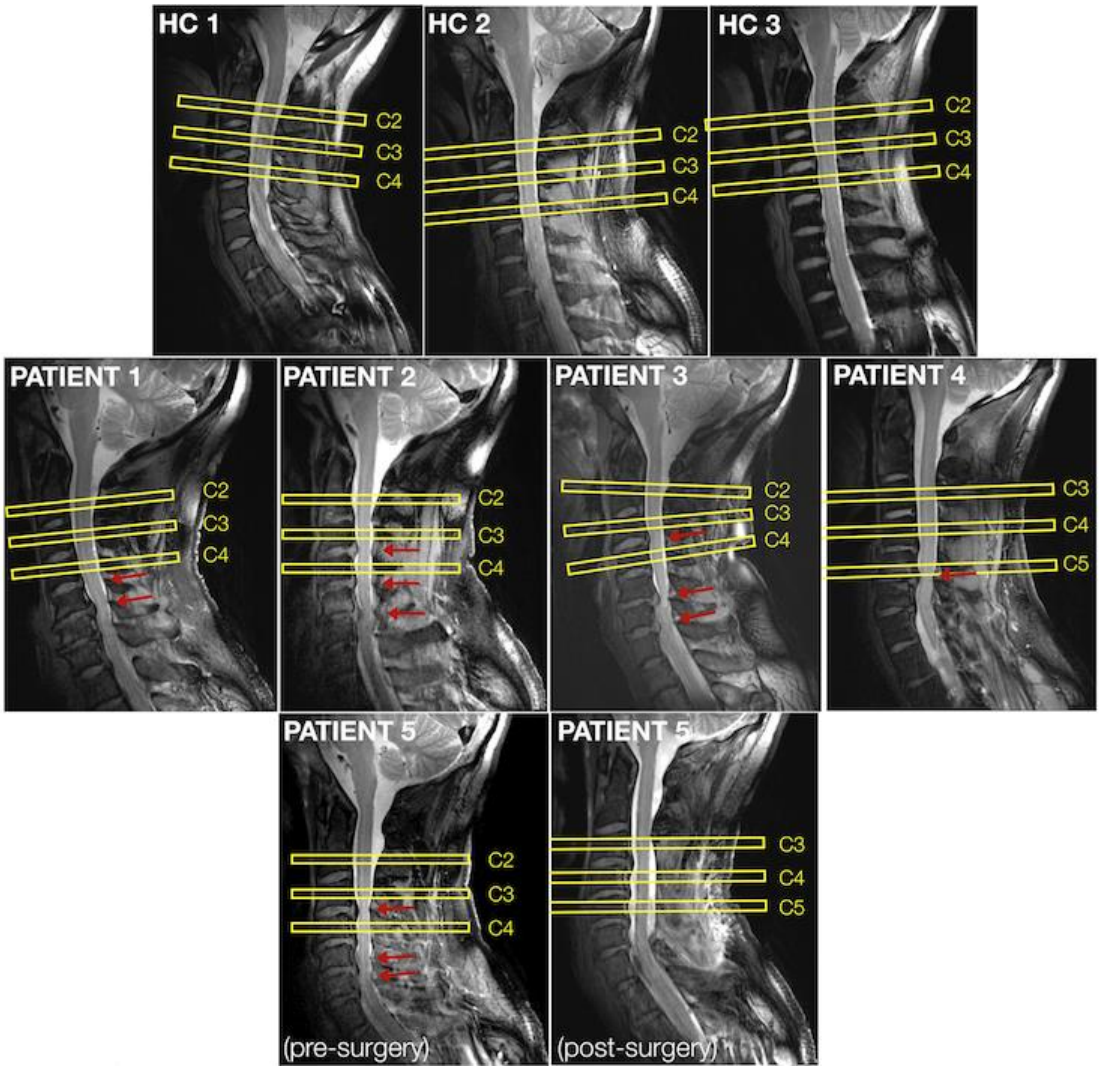

Fig. S1 - Sagittal anatomical images (2D turbo spinecho, 0.6×0.6mm2 in-plane resolution) and positions of the 2D transversal slices (yellow) for perfusion imaging of the cervical spinal cord of each participant, healthy volunteers (HC) and patients. Red arrows indicate spinal cord compressions.

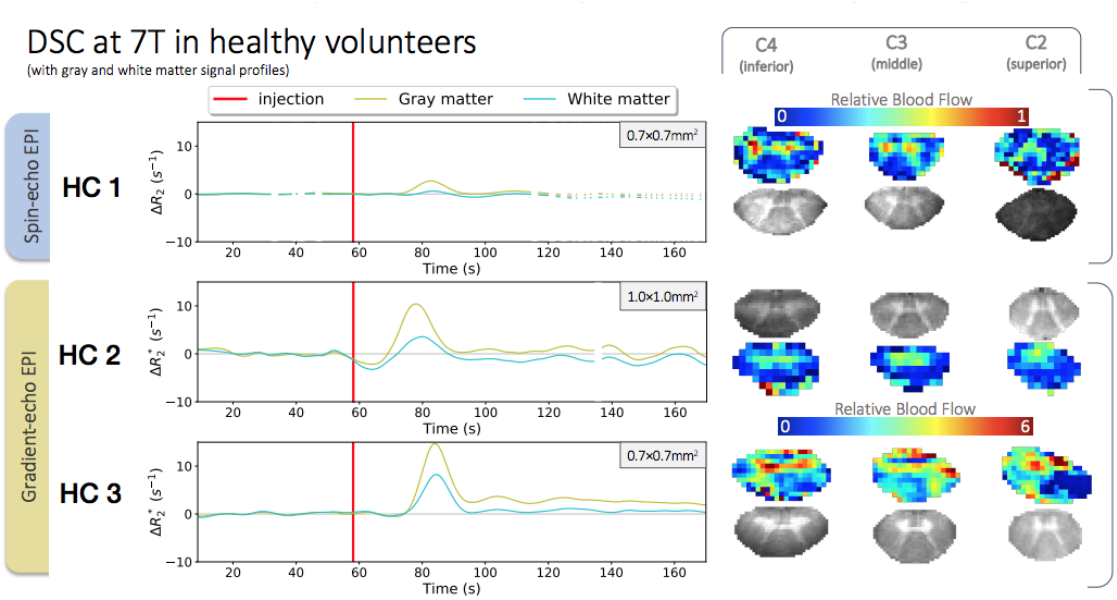

Fig. S2 - This figure is similar to Figure 4 of the main manuscript, except that the signal-time profiles showed on the left side correspond to the average signal along time within gray and white matter. Bolus peak was clearly higher in gray matter compared to white matter but timings were similar. Regions of interest were defined manually based on relative blood flow and blood volume maps, discarding voxels affected by partial voluming at the edge of the cord. As in Figure 3, on the right side, the relative blood flow maps resulting from a voxel-wise processing are presented alongside the corresponding anatomical scans (2D multi-echo gradient-echo FLASH with 0.4×0.4mm2 in-plane resolution) for gray and white matter localization. Spin-echo EPI was tested in one healthy volunteer with high in-plane resolution (0.7×0.7mm2) while gradient-echo EPI was tested in two healthy volunteers, with high and lower (1.0×1.0mm2) in-plane resolution.

9. Acknowledgements

The authors would like to thank Sylviane Confort-Gouny, Véronique Gimenez, Lauriane Pini, Claire Costes, Patrick Viout, Muriel Juge-Boulogne and Virginie Véla for study logistics.

This project received funding from the European Union's Horizon 2020 research and innovation program under the Marie Skłodowska-Curie grant agreement #713750. Also, it was carried out with financial support from the Regional Council of Provence-Alpes-Côte d'Azur and with financial support from the A*MIDEX (#ANR-11-IDEX-0001-02), funded by the Investissements d'Avenir project funded by the French Government, managed by the French National Research Agency (ANR).
This work was performed within a laboratory member of France Life Imaging network (#ANR-11-INBS-0006), supported by the following funding sources: 7T-AMI-ANR-11-EQPX-0001, A*MIDEX-EI-13-07-130115-08.38-7T-AMISTART and CNRS (Centre National de la Recherche Scientifique).

10. References

1. Schubert M. Natural Course of Disease of Spinal Cord Injury. In: Weidner N, Rupp R, Tansey KE, eds. *Neurological Aspects of Spinal Cord Injury*. Springer International Publishing; 2017:77-105. doi:10.1007/978-3-319-46293-6_4

2. Gilmor ML, Rouse S, Heilman CJ, Nash N, Levey A. Receptor fusion proteins and analysis. In: Ariano M, ed. *Receptor Localization*. Vol 19. WILEY; 1998:75-90.

3. Beattie MS, Farooqui AA, Bresnahan JC. Review of Current Evidence for Apoptosis After Spinal Cord Injury. *J Neurotrauma*. 2000;17(10):915-925. doi:10.1089/neu.2000.17.915

4. Kalsi-Ryan S, Karadimas SK, Fehlings MG. Cervical Spondylotic Myelopathy: The Clinical Phenomenon and the Current Pathobiology of an Increasingly Prevalent and Devastating Disorder. *The Neuroscientist*. 2012;19(4):409-421. doi:10.1177/1073858412467377

5. Alsop DC, Detre JA, Golay X, et al. Recommended implementation of arterial spin-labeled perfusion MRI for clinical applications: A consensus of the ISMRM perfusion study group and the European consortium for ASL in dementia: Recommended Implementation of ASL for Clinical Applications. *Magn Reson Med*. 2015;73(1):102-116. doi:10.1002/mrm.25197

6. Le Bihan D, Breton E, Lallemand D, Aubin ML, Vignaud J, Laval-Jeantet M. Separation of diffusion and perfusion in intravoxel incoherent motion MR imaging. *Radiology*. 1988;168(2):497-505. doi:10.1148/radiology.168.2.3393671

7. Aracki-Trenkic A, Law-ye B, Radovanovic Z, Stojanov D, Dormont D, Pyatigorskaya N. ASL perfusion in acute ischemic stroke: The value of CBF in outcome prediction. *Clin Neurol Neurosurg*. 2020;194:105908. doi:10.1016/j.clineuro.2020.105908

8. Turnbull IM. Blood Supply of the Spinal Cord: Normal and Pathological Considerations. *Neurosurgery*. 1973;20(CN_suppl_1):56-84. doi:10.1093/neurosurgery/20.CN_suppl_1.56

9. Tator CH, Koyanagi I. Vascular mechanisms in the pathophysiology of human spinal cord injury. *J Neurosurg*. 1997;86(3):483-492. doi:10.3171/jns.1997.86.3.0483

10. Duhamel G, Callot V, Cozzone PJ, Kober F. Spinal cord blood flow measurement by arterial spin labeling. *Magn Reson Med*. 2008;59:846-854. doi:10.1002/mrm.21567

11. Verma T, Cohen-Adad J. Effect of respiration on the B0 field in the human spinal cord at 3T: Effect of Respiration on B0 Field in Human Spinal Cord. *Magn Reson Med*. 2014;72(6):1629-1636. doi:10.1002/mrm.25075

12. Vannesjo SJ, Miller KL, Clare S, Tracey I. Spatiotemporal characterization of breathing-induced B0 field fluctuations in the cervical spinal cord at 7T. *NeuroImage*. 2018;167:191-202. doi:10.1016/j.neuroimage.2017.11.031

13. Lu H, Law M, Ge Y, et al. Quantitative measurement of spinal cord blood volume in humans using vascular-space-occupancy MRI. *NMR Biomed*. 2008;21(3):226-232. doi:10.1002/nbm.1185

14. Parkes Laura M., Rashid Waqar, Chard Declan T., Tofts Paul S. Normal cerebral perfusion measurements using arterial spin labeling: Reproducibility, stability, and age and gender effects. *Magn Reson Med*. 2004;51(4):736-743. doi:10.1002/mrm.20023

15. Girard OM, Callot V, Robert B, Cozzone PJ, Duhamel G. Perfusion MRI of the Human Cervical Spinal Cord using Arterial Spin Labeling. In: *Proceedings of the 21st Annual Meeting of the International Society for Magnetic Resonance in Medicine*. ; 2013:0349.

16. Nair G, Hu XP. Perfusion Imaging of the Human Cervical Spinal Cord. In: *Proceedings of the 19th Annual Meeting of the International Society for Magnetic Resonance in Medicine*. ; 2010:4083.

17. Lévy S, Rapacchi S, Massire A, et al. Intravoxel Incoherent Motion at 7 Tesla to quantify human spinal cord perfusion: Limitations and promises. *Magn Reson Med*. Published online February 14, 2020:mrm.28195. doi:10.1002/mrm.28195

18. Donahue MJ, Hua J, Pekar JJ, van Zijl PCM. Effect of inflow of fresh blood on vascular-space-occupancy (VASO) contrast. *Magn Reson Med*. 2009;61(2):473-480. doi:10.1002/mrm.21804

19. Scouten A, Constable RT. VASO-based calculations of CBV change: Accounting for the dynamic CSF volume. *Magn Reson Med*. 2008;59(2):308-315. doi:10.1002/mrm.21427

20. Vargas MI, Delattre BMA, Boto J, et al. Advanced magnetic resonance imaging (MRI) techniques of the spine and spinal cord in children and adults. *Insights Imaging*. 2018;9(4):549-557. doi:10.1007/s13244-018-0626-1

21. Fehlings MG, Skaf G. A review of the pathophysiology of cervical spondylotic myelopathy with insights for potential novel mechanisms drawn from traumatic spinal cord injury. *Spine*. 1998;23(24):2730-2737.

22. Ellingson BM, Woodworth DC, Leu K, Salamon N, Holly LT. Spinal Cord Perfusion MR Imaging Implicates Both Ischemia and Hypoxia in the Pathogenesis of Cervical Spondylosis. *World Neurosurg*. 2019;128:e773-e781. doi:10.1016/j.wneu.2019.04.253

23. Staff News Brief. Siemens obtains first CE approval for ultra-high-field 7T MR scanner. *Appl Radiol*. https://appliedradiology.com/articles/siemens-obtains-first-ce-approval-for-ultra-high-field-7t-mr-scanner. Published October 25, 2017. Accessed April 12, 2020.

24. Polimeni JR, Uludağ K. Neuroimaging with ultra-high field MRI: Present and future. *Neuroimaging Ultra-High Field MRI Present Future*. 2018;168:1-6. doi:10.1016/j.neuroimage.2018.01.072

25. Kraff O, Quick HH. 7T: Physics, safety, and potential clinical applications: 7T: Physics, Safety, Applications. *J Magn Reson Imaging*. 2017;46(6):1573-1589. doi:10.1002/jmri.25723

26. Rohrer M, Bauer H, Mintorovitch J, Requardt M, Weinmann H-J. Comparison of Magnetic Properties of MRI Contrast Media Solutions at Different Magnetic Field Strengths: *Invest Radiol*. 2005;40(11):715-724. doi:10.1097/01.rli.0000184756.66360.d3

27. Noebauer-Huhmann IM, Kraff O, Juras V, et al. MR Contrast Media at 7Tesla - Preliminary Study on Relaxivities. In: *Proceedings of the 16th Annual Meeting of the International Society for Magnetic Resonance in Medicine*. ; 2008:1457.

28. Massire A, Taso M, Besson P, Guye M, Ranjeva J-P, Callot V. High-resolution multi-parametric quantitative magnetic resonance imaging of the human cervical spinal cord at 7T. *NeuroImage*. 2016;143:58-69. doi:10.1016/j.neuroimage.2016.08.055

29. Kellner E, Dhital B, Kiselev VG, Reisert M. Gibbs-ringing artifact removal based on local subvoxel-shifts. *Magn Reson Med*. 2016;76(5):1574-1581. doi:10.1002/mrm.26054

30. Avants BB, Tustison NJ, Song G, Cook PA, Klein A, Gee JC. A reproducible evaluation of ANTs similarity metric performance in brain image registration. *NeuroImage*. 2011;54:2033-2044. doi:http://dx.doi.org/10.1016/j.neuroimage.2010.09.025

31. Maggioni M, Katkovnik V, Egiazarian K, Foi A. Nonlocal Transform-Domain Filter for Volumetric Data Denoising and Reconstruction. *IEEE Trans Image Process*. 2013;22(1):119-133. doi:10.1109/TIP.2012.2210725

32. Andersson JLR, Skare S, Ashburner J. How to correct susceptibility distortions in spin-echo echo-planar images: application to diffusion tensor imaging. *NeuroImage*. 2003;20(2):870-888. doi:10.1016/S1053-8119(03)00336-7

33. Polimeni JR, Bhat H, Witzel T, et al. Reducing sensitivity losses due to respiration and motion in accelerated echo planar imaging by reordering the autocalibration data acquisition: Reducing Losses in Accelerated EPI with FLEET-ACS. *Magn Reson Med*. 2016;75(2):665-679. doi:10.1002/mrm.25628

34. Talagala SL, Sarlls JE, Liu S, Inati SJ. Improvement of temporal signal-to-noise ratio of GRAPPA accelerated echo planar imaging using a FLASH based calibration scan: Temporal SNR of GRAPPA Accelerated EPI. *Magn Reson Med*. 2016;75(6):2362-2371. doi:10.1002/mrm.25846

35. van Gelderen P, de Zwart JA, Starewicz P, Hinks RS, Duyn JH. Real-time shimming to compensate for respiration-induced B0 fluctuations. *Magn Reson Med*. 2007;57(2):362-368. doi:10.1002/mrm.21136

36. Boer VO, vd Bank BL, van Vliet G, Luijten PR, Klomp DWJ. Direct B0 field monitoring and real-time B0 field updating in the human breast at 7 tesla. *Magn Reson Med*. 2012;67(2):586-591. doi:10.1002/mrm.23272

37. Bianciardi M, Polimeni JR, Setsompop K, Eichner C, Bilgic B, Wald LL. Evaluation of dynamic off-resonance correction of respiratory instability in MRI signals for high-order spherical harmonic basis set and multivariate modeling of respiratory sources. In: *Proc. Int. Soc. Magn. Reson. Med. 22*. ; 2014:1623.

38. Irwan R, Lubbers DD, van der Vleuten PA, Kappert P, Götte MJW, Sijens PE. Parallel imaging for first-pass myocardial perfusion. *Magn Reson Imaging*. 2007;25(5):678-683. doi:10.1016/j.mri.2006.10.012

39. Figley CR, Stroman PW. Investigation of human cervical and upper thoracic spinal cord motion: Implications for imaging spinal cord structure and function. *Magn Reson Med*. 2007;58(1):185-189. doi:10.1002/mrm.21260

40. Figley CR, Yau D, Stroman PW. Attenuation of Lower-Thoracic, Lumbar, and Sacral Spinal Cord Motion: Implications for Imaging Human Spinal Cord Structure and Function. *Am J Neuroradiol*. 2008;29(8):1450-1454. doi:10.3174/ajnr.A1154

41. Duhamel G, Callot V, Decherchi P, et al. Mouse lumbar and cervical spinal cord blood flow measurements by arterial spin labeling: Sensitivity optimization and first application. *Magn Reson Med*. 2009;62:430-439. doi:10.1002/mrm.22015

42. Zhang B, Seifert AC, Kim J, Borrello J, Xu J. 7 Tesla 22-channel wrap-around coil array for cervical spinal cord and brainstem imaging: 7T Cervical Spinal Cord Coil. *Magn Reson Med*. 2017;78(4):1623-1634. doi:10.1002/mrm.26538

43. Topfer R, Foias A, Stikov N, Cohen-Adad J. Real-time correction of respiration-induced distortions in the human spinal cord using a 24-channel shim array: Real-Time ΔB_0 Shimming in the Spinal Cord. *Magn Reson Med*. 2018;80(3):935-946. doi:10.1002/mrm.27089

44. Feinberg DA, Setsompop K. Ultra-fast MRI of the human brain with simultaneous multi-slice imaging. *J Magn Reson*. 2013;229:90-100. doi:10.1016/j.jmr.2013.02.002

45. Preibisch C, Castrillón G. JG, Bührer M, Riedl V. Evaluation of Multiband EPI Acquisitions for Resting State fMRI. Zhan W, ed. *PLOS ONE*. 2015;10(9):e0136961. doi:10.1371/journal.pone.0136961